Arch. Metall. Mater. **65** (2020), 3, 1073-1080

DOI: 10.24425/amm.2020.133220

TAE-HYUN PARK[1], MIN-SEOK BAEK[1], YONGHO SOHN[2,3], KEE-AHN LEE[1*]

EFFECT OF POST-HEAT TREATMENT ON THE WEAR PROPERTIES OF AlSi10Mg ALLOY MANUFACTURED BY SELECTIVE LASER MELTING

Microstructure and wear property of AlSi10Mg alloy manufactured by selective laser melting (SLM) were investigated. Also, the effect of post heat treatment on the mechanical and wear properties was examined. Two kinds of heat treatments (direct aging (DA) and T6) were separately conducted to SLM AlSi10Mg alloy. As-built alloy had a cellular structure formed inside the molten pool. Eutectic Si was also observed at the cellular boundary in as-built alloy. After DA heat treatment, the cellular structure still remained, and a large amount of nano-size Si particles were newly formed inside the cell structure. Both molten pool and cellular structure disappeared, and the size of Si increased in T6 alloy. The values of Vickers hardness measured as 139.4 HV (DA alloy), 128.0 HV (As-built alloy) and 85.1 HV (T6 alloy), respectively. However, concerning to wear property, T6 alloy showed better wear resistance than other alloys. The correlation between microstructure and wear mechanism of SLM AlSi10Mg alloy was also discussed.

Keywords: Selective Laser Melting (SLM), AlSi10Mg, Heat treatment, Microstructure, Wear

1. Introduction

Among Al-based alloys, AlSi10Mg alloy has a low thermal expansion coefficient, high specific strength and excellent mechanical properties. Especially, AlSi10Mg is an alloy that contains Si phase, which is known to give outstanding wear resistance [1]. Due to such characteristics, this alloy is commonly used in automotive applications such as pistons and engine blocks [1,2]. Furthermore, application of AlSi10Mg alloy in the aircraft and ship industries is also being explored.

AlSi10Mg alloy was mainly manufactured by casting. However, the casting process has a slow cooling rate of approximately 10^2 ℃/s or less, and It is also known that the size of eutectic Si tends to be coarse easily. [3]. In addition, casting forms secondary dendrite structures that hinder the mechanical properties and wear resistance of the alloy.

Recently, there have been attempts to manufacture AlSi10Mg alloy using additive manufacturing (AM), and such attempts have been garnering great interest [4]. Among the various AM processes, selective laser melting (SLM) is capable of achieving fast cooling rate (10^6 ℃/s-10^8 ℃/s), and it is being reported as the most ideal process to manufacture Al alloys [5]. Due to its fast cooling rate, SLM forms unique and fine microstructures such as its molten pool and cellular structure. These unique microstructures are reported to make contributions to improving the alloy's mechanical properties such as hardness, tensile strength and compression [6,7].

However, Al-based alloys manufactured by SLM can have defects such as pores [8]. Such defects cause microstructural instability, which in turn has a harmful influence on the alloy's mechanical properties [9]. As a result, many past studies have proposed post-heat treatment to resolve the issues caused by the defects [10,11]. And then, T6 heat treatment is a precipitation hardening heat treatment that has been used on AM materials as well as commercial Al-Si wrought materials. However, unlike commercial wrought materials, AlSi10Mg alloy manufactured by SLM was reported to suffer a decrease in mechanical properties after T6 heat treatment [12]. The reason why SLM AlSi10Mg alloy's mechanical properties decrease after T6 heat treatment has not been clearly identified.

AlSi10Mg alloy is commonly used in automobile and aircraft parts, and wear resistance is one of its most critical physical properties [13]. Eutectic Si found in commercial wrought AlSi10Mg materials has a good influence on the alloy's wear

[1] INHA UNIVERSITY, DEPARTMENT OF MATERIALS SCIENCE AND ENGINEERING, 22212, INCHEON, REPUBLIC OF KOREA
[2] UNIVERSITY OF CENTRAL FLORIDA, ADVANCED MATERIALS PROCESSING AND ANALYSIS CENTER, ORLANDO, USA
[3] UNIVERSITY OF CENTRAL FLORIDA, DEPARTMENT OF MATERIALS SCIENCE AND ENGINEERING, ORLANDO, USA

* Corresponding author: keeahn@inha.ac.kr

resistance. In addition, Al_2O_3 formed on the wear surface during wear plays the act of a solid lubricant that contributes to reducing wear loss [14]. However, AlSi10Mg alloy manufactured by SLM is reported to form a microstructure that is different from the microstructure of conventional AlSi10Mg material [15]. Despite this, no study has looked into the wear resistance of AlSi10Mg alloy manufactured by SLM.

In this study, AlSi10Mg alloy was manufactured using SLM, and its microstructure and wear properties were examined. Also, the effect of post-heat treatment on wear resistance and wear behavior was investigated.

2. Experimental Method

Selective laser melting (SLM) was used in scan pattern of hatch type to manufacture a bar-shape AlSi10Mg alloy 10 mm×10 mm×100 mm in size. To identify the chemical composition of AlSi10Mg alloy, X-ray fluorescence (XRF, ZSX Primus II) analysis was performed, and the results are listed in Table 1. The manufactured alloy was confirmed to have a chemical composition that fell in the range of standard compositions.

TABLE 1

Chemical compositions of AlSi10Mg in XRF Results (wt. %)

Element	Al	Si	Mg	Fe	Total
AlSi10Mg	89.9%	9.6%	0.3%	0.2%	100%

Post-heat treatment was performed using a box furnace at room temperature, and the conditions used are shown in Fig. 1. AlSi10Mg alloy manufactured by SLM is reported to be in a non-equilibrium state where large amounts of Si are molten into the Al matrix [16]. As a result, post-heat treatment (precipitation hardening heat treatment) was performed under two conditions. The first condition was direct aging (DA) heat treatment, which only performs aging at 180°C for 6 hours while omitting solution heat treatment. The second heat treatment was T6 heat treatment, which is used on commercial wrought Al-Si alloys. T6 heat treatment was performed by applying 2 hours of solution heat treatment at 520°C, then applying water cooling, and conducting 6 hours of aging at 180°C.

In order to perform phase analysis and microstructural observation of AlSi10Mg alloy, pretreatment was applied. First, the specimen was ground using a polisher with #400 ~ #4000, and final polishing was applied with 1 μm diamond paste and colloidal silica of 0.04 μm. X-ray diffraction (XRD, ULTIMA IV, scan speed 4°/min and 2-theta 25° ~ 105°) equipment was used for phase analysis. Microstructural observations were made using an optical microscope (OM), scanning electron microscope (SEM, TESCAN; VEGA II LMU), field emission scanning electron microscope (FE-SEM, FEI COMPANY; QUANTA 200F) and electron back-scattered diffraction (EBSD, OXFORD; Nordlys nano detector, step size 200 nm, 15 kV) equipment. The etching solution used was modified Keller's reagent (190 ml H_2O, 5 ml HNO_3, 3 ml HCl and 2 ml HF).

Vickers hardness test was performed at room temperature. The hardness was measured using Vickers hardness (Akashi, AVK-C100) equipment. A wear test was performed to identify the wear resistance property of the alloy. The ball-on-disk method was applied with no lubrication at room temperature. In addition, a rotation radius of 3 mm, rotation speed of 80.2 RPM, straight rate of 25.2 mm/s and vertical load of 10 N were employed. The ball used for the wear test was made of SAE 52100 (ASTM; bearing steel) with 5.556 mm diameter.

3. Results and discussion

3.1. Microstructure characteristics of SLMed AlSi10Mg Alloys with post-heat treatments

The microstructures of AlSi10Mg alloy manufactured by SLM (as-built) and alloys with post-heat treatment applied (DA & T6) were observed macroscopically using an optical

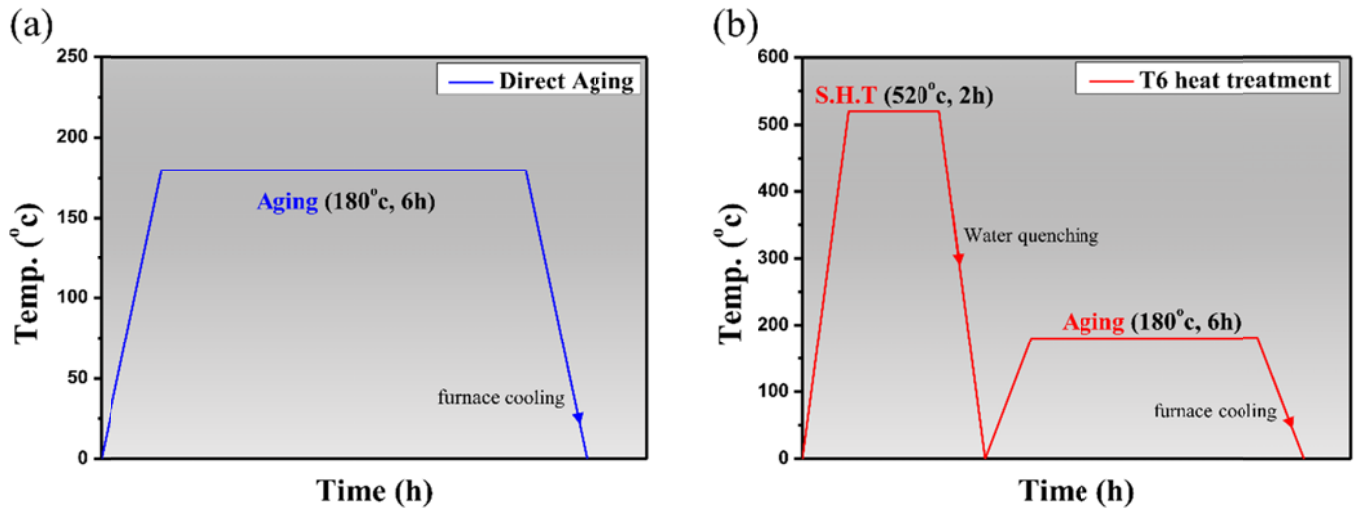

Fig. 1. Schematic schedule of heat treatment: (a) direct aging (DA) and (b) T6 Heat treatment

microscope (OM), and the results are shown in Fig. 2. Molten pools were found in the as-built alloy (Fig. 2a), and structures were similar to the microstructure of alloys manufactured by SLM. The above-mentioned molten pool measured 76.3 µm and 170.8 µm in width and height, respectively. The alloy with direct aging (DA) heat treatment applied (Fig. 2b) also maintained the molten pools found in the as-built alloy. Even though the DA heat treatment temperature was approximately 180 °C, which is not significantly low, the fact that the molten pools in the as-built alloy did not disappear is an interesting finding. The width and height of the molten pools found in the DA alloy measured 80.3 µm and 164.4 µm, respectively, which are similar to those in the as-built alloy. Unlike the other two alloys, no molten pools were found in the case of the alloy with T6 heat treatment applied (Fig. 2c). In addition, black phases were formed throughout the T6 alloy, and the overall structure was somewhat different from the other two alloys.

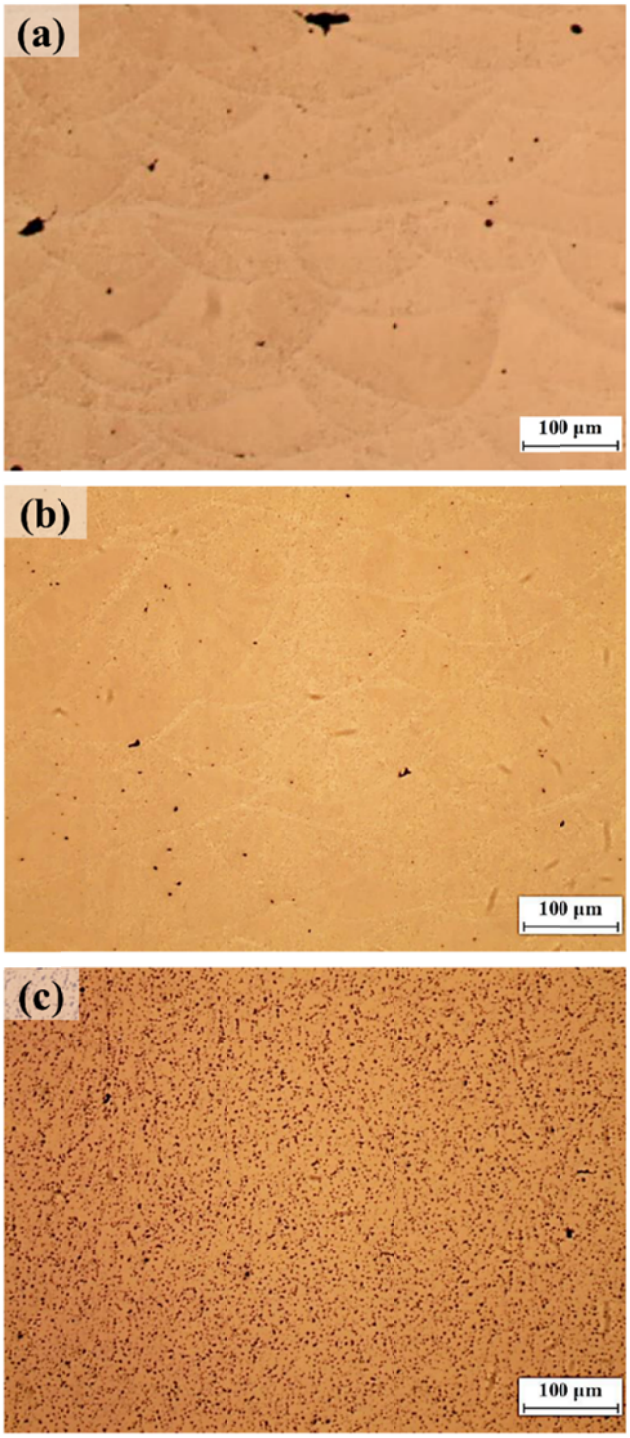

Fig. 2. OM images showing the microstructure of AlSi10Mg alloy: (a) as-built, (b) DA and (c) T6 alloys

Fig. 3 is the XRD analysis results of the three alloys. Si phase were found with Al phase in all three alloys, and no additional precipitation phases [17] were detected. In a detail look at the XRD results, the peak intensity of the Si phase in T6 alloy was higher than the two other alloys. This is suspected to be due to additionally precipitated Si (black phases in Fig. 2c) as a result of the solution heat treatment of T6 heat treatment, which in turn increased Si ratio.

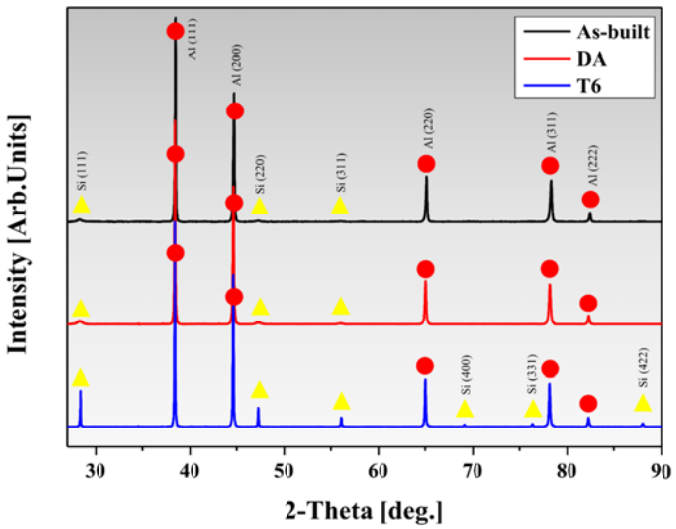

Fig. 3. XRD patterns of SLM-ed AlSi10Mg alloys (as-built, DA and T6 alloys)

Fig. 4 is the observation results of the internal structures of the as-built and heat treated (DA, T6) alloys. The as-built alloy had a cellular structure within the molten pool, and its size measured 0.63 µm. In addition, eutectic Si was found at the cellular structure boundary of the as-built alloy. In the case of the DA alloy (Fig. 4b), a cellular structure similar to that of the as-built alloy was observed, and its size was similar to the as-built alloy, but measured slightly larger (0.69 µm). Meanwhile, within the cellular structure, a large number of nano-sized Si particles precipitated. This is suspected to be the solid solution Si inside the Al matrix precipitating in nano size due to the aging heat treatment performed at approximately 180°C. On the other hand, no cellular structure was observed in the T6 alloy (Fig. 4c). In addition, T6 alloy had relatively coarse Si phases of 2.35 µm.

EBSD analysis was performed to identify the grain shape and size of the as-built and heat treated (DA, T6) alloys, and the results are shown in Fig. 5. Inverse pole figure (IPF) identified grains of the as-built alloy (Fig. 5a) to be columnar, and their size measured 9.09 µm. In general, the grains of SLM-manufactured

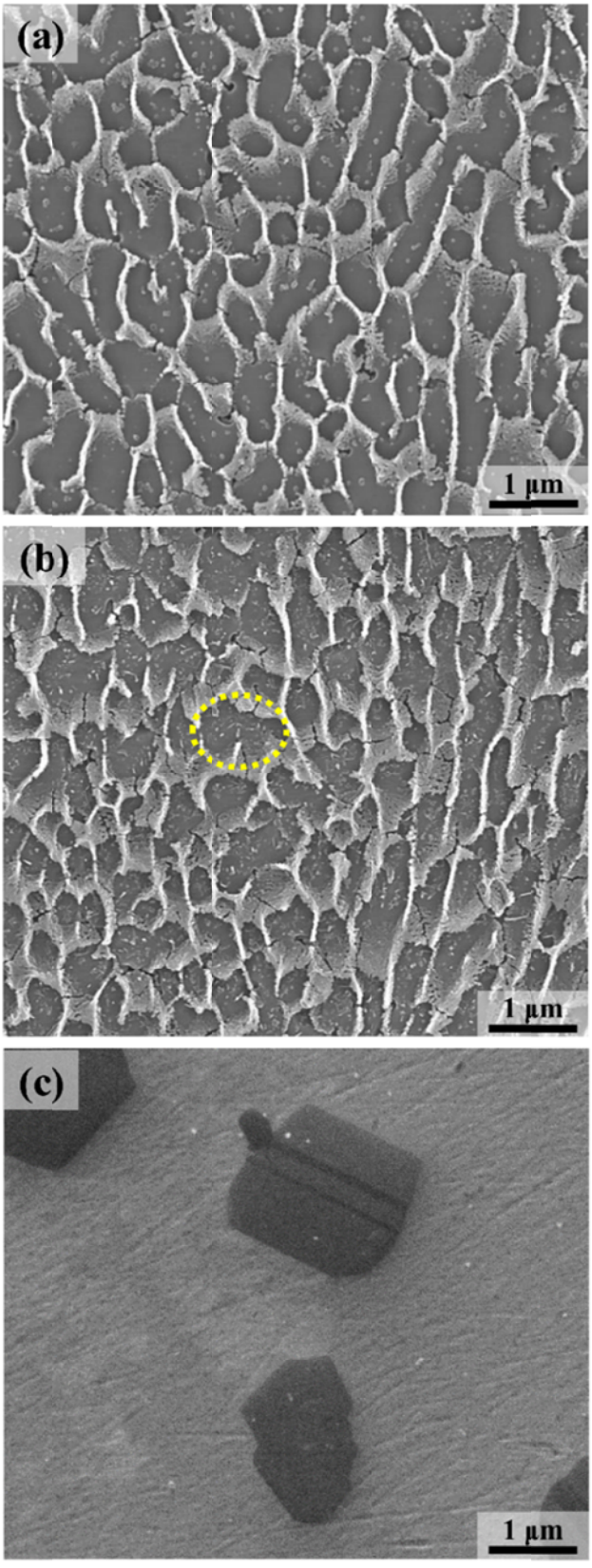

Fig. 4. SEM images showing the microstructure of AlSi10Mg alloy: (a) as-built, (b) DA and (c) T6 alloys

materials are reported to assume a columnar shape as they develop in the building direction (Z axis) [18]. The DA heat treated alloy maintained a columnar grain shape similar to the as-built alloy, but its size was slightly larger at approximately 10.37 µm. On the other hand, the T6 alloy developed coarse grains, unlike the other two alloys (as-built, DA), and the size measured 21.68 µm. A kernel average misorientation (KAM) map of the three alloys was also analyzed. The KAM values of the as-built alloy (Fig. 5d) were insignificant, and KAM values appeared to have localized into some grain boundaries and columnar boundaries within grains. Meanwhile, the KAM values of the DA alloy (Fig. 5e) were higher than the as-built alloy, and the KAM values were evenly distributed throughout. This is suspected to be due to the nano-sized Si particles formed by the DA heat treatment. A. Hadadzadeh et al. [19] reported that if Si precipitates, dislocations entangle with the Si precipitate interface due to the difference in thermal expansion coefficient between Si and Al matrix. The KAM values in T6 alloy (Fig. 5f) were confirmed to be concentrated in local areas. The distribution size of KAM values was approximately 2 µm, and considering the size, this area can be deduced to be the surrounding areas of Si phase precipitated on the grain boundary.

3.2. Wear properties of SLM AlSi10Mg alloys with post-heat treatments

Before performing the wear test, the Vickers hardness of the three alloys was measured, and the results are listed in Table 2. The hardness of the three alloys was 128.0 HV (as-built), 139.4 HV (DA) and 85.1 HV (T6), respectively, and hardness was the highest in the DA alloy. This is suspected to be due to the nano-sized Si precipitated after DA heat treatment. On the other hand, despite precipitation hardening heat treatment being performed, the hardness of T6 alloy was lower than the hardness of the as-built alloy. This might be attributable to the fact that the solution heat treatment of T6 alloy caused the molten pool and cellular structure to disappear, leading to the Al matrix becoming softer.

Fig. 6 shows the ball-on-disc wear results. The wear properties of the three alloys are expressed in wear loss (g), and the alloys measured 0.0185 g (as-built), 0.0178 g (DA) and 0.0156 g (T6). This indicated that the wear loss of T6 alloy decreased by 15.7 % compared to the as-built alloy. In other words, T6 alloy had greater wear properties compared to the other two alloys. In general, wear properties are reported to be greater as the hardness and strength of the material increase [20]. However, in this study, T6 alloy had the lowest hardness value, but the highest wear resistance value.

TABLE 2

Quantitative Vickers hardness values: as-built, DA and T6 alloys

Alloy	As-built	DA	T6
Vickers Hardness [HV]	128.0 ± 12.0	139.4 ± 10.9	85.1 ± 4.1

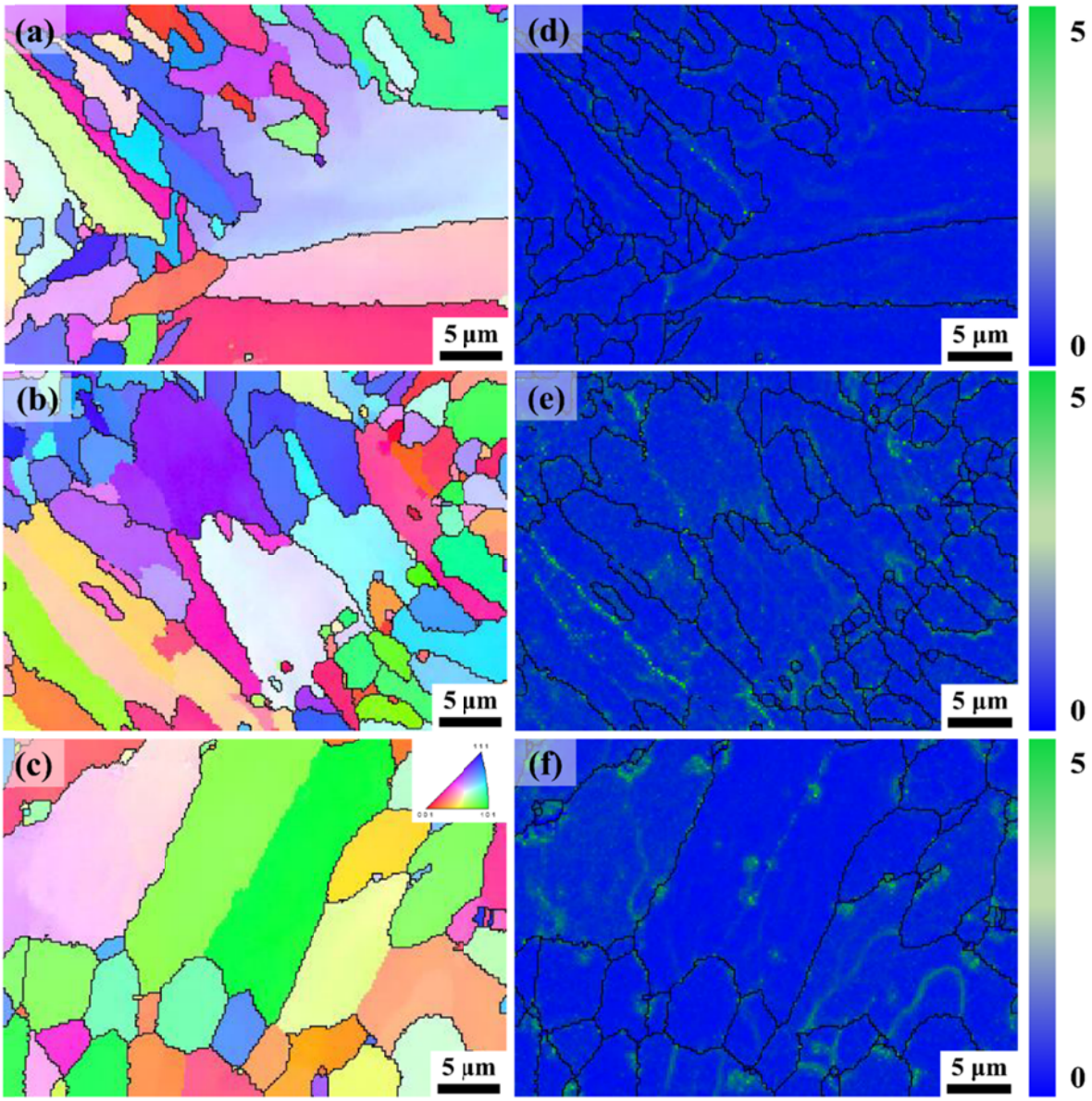

Fig. 5. EBSD analysis of SLM-ed AlSi10Mg alloy: inverse pole figure (IPF) maps [(a) as-built, (b) DA alloy and (c) T6 alloy] and kernel average misorientation maps [(d) as-built, (e) DA alloy and (f) T6 alloy]

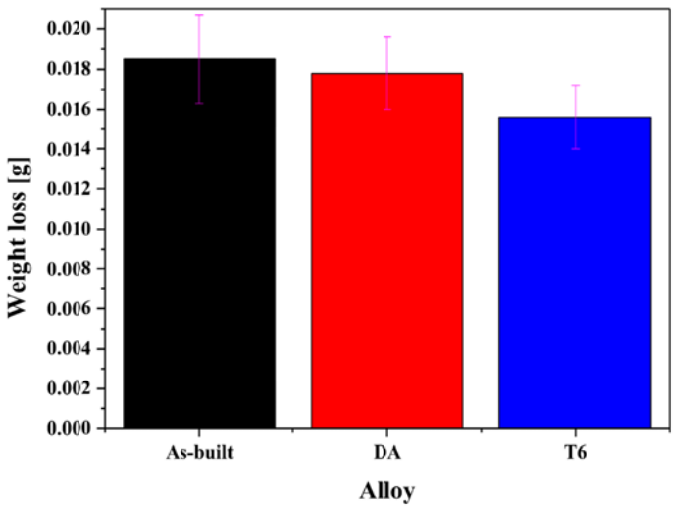

Fig. 6. Weight loss values for various alloys in dry condition

3.3. Wear behaviors of SLM AlSi10Mg alloys with post-heat treatments

In order to analyze the unique wear behavior described above, the wear surfaces of the three alloys were observed (Fig. 7). In low magnification observation of the wear surfaces, the as-built and DA alloys had a hair cuticle-like shape (red arrow). In addition, the width of the cuticles found in the two alloys was smaller in the as-built alloy. In the case of the T6 alloy, the macroscopic wear surface featured grind wear behavior, which is a typical Al-Si alloy wear surface.

In high magnification observation of the wear surfaces, nano-sized Si particles were found between the cuticles of the as-built alloy (Fig. 7d). This indicated that the nano-sized particles in the as-built alloy created debris as they failed to execute their role as a wear resistor during the wear. In general, Si in Al-Si

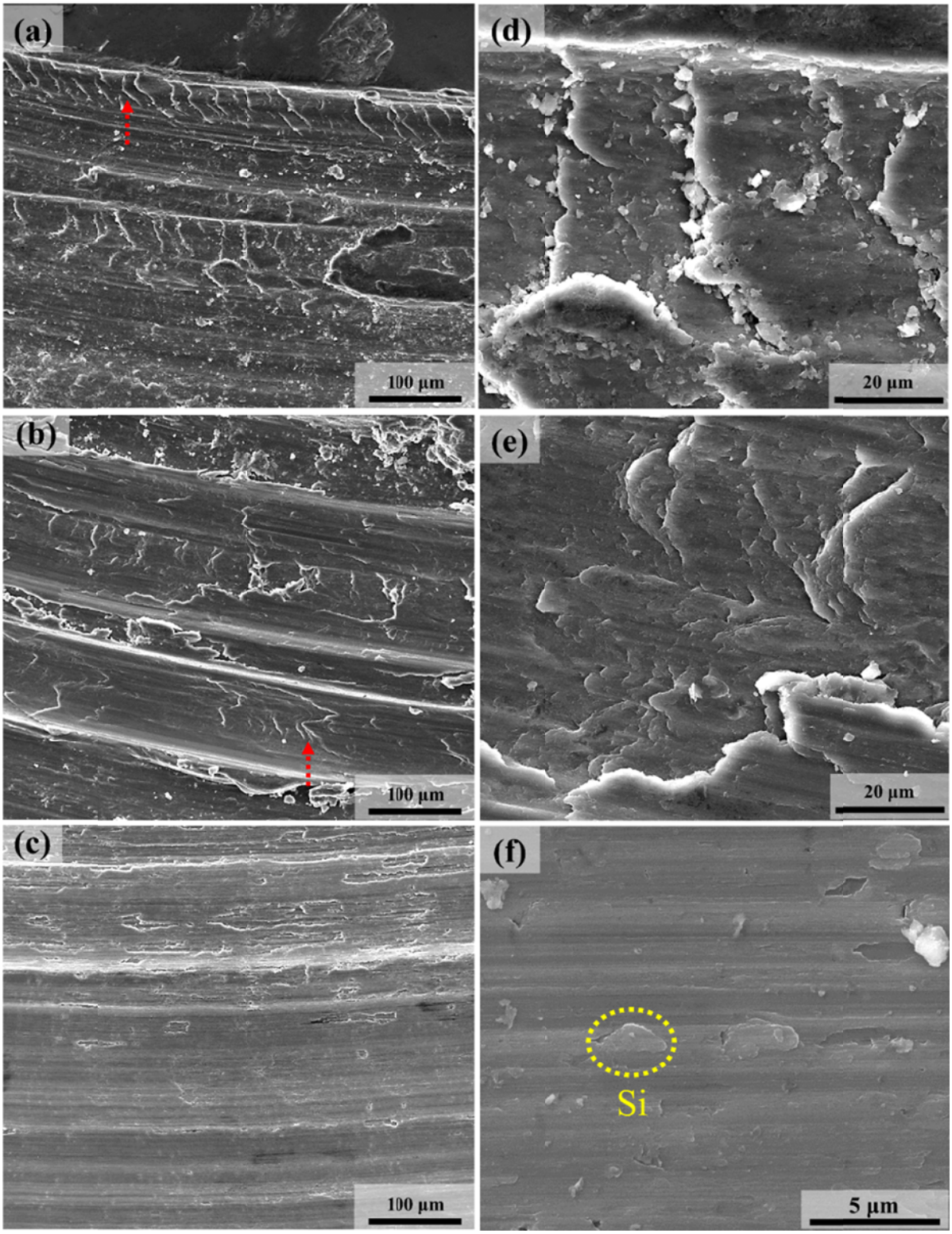

Fig. 7. SEM images of the wear surface: (a,d) as-built, (b,e) DA and (c,f) T6 alloys

alloy is known to be significantly hard, which allows it to act as a wear resistor [21]. In addition, it is also reported that adhesion with the Al matrix plays a critical role in Si to fully execute its role as a wear resistor [22]. However, the nano-sized Si particles in the AlSi10Mg alloy manufactured by SLM have low adhesion with the Al matrix, so this characteristic is suspected to cause the Si precipitated from the Al matrix to form debris. High magnification observation of the DA alloy (Fig. 7e) confirmed that nano-sized Si particles are present between cuticles, as in the as-built alloy. However, its Si content was relatively less. This is suspected to be due to the slightly greater adhesion between the nano-sized Si and the Al matrix achieved through DA heat treatment. As in the initial microstructure (Fig. 5f), the KAM values of DA alloy were evenly distributed throughout the Al

matrix, and this was considered to be due to the precipitated nano-sized Si particles. According to H. J. Kim et al. [23], if Si precipitates after applying T6 heat treatment to Al-Si alloy, the dislocation density of the surrounding areas increases. The high adhesion between Al and Si can be understood to be the result of the high dislocation density at the Si interface. So, the greater adhesion between nano-sized Si particles and the Al matrix of the DA alloy is suspected to suppress debris formation compared to the as-built alloy. In addition, less debris formation can be interpreted to result in the narrower cuticle width and less wear loss. High magnification observation of the T6 wear surface (Fig. 7f), the precipitated Si due to T6 heat treatment was not removed from the Al matrix and sufficiently executed its role as a wear resistor. In addition, the Si particles, approximately 2 μm in size, contribute to the reduction of wear loss as they induce grinding wear. The reason why Si phases are not detached in T6 alloy can be explained with the KAM values concentrated around Si (Fig. 5f). In other words, solution heat treatment + T6 aging alloy will be able to precipitate fine Si phases while strengthening its adhesion with the Al matrix.

In order to further identify the wear behaviors observed in the above-mentioned alloys, the wear surface roughness was measured using a 3D profiler, and Fig. 8 shows the results of measurement. The wear progression surface width of the as-built

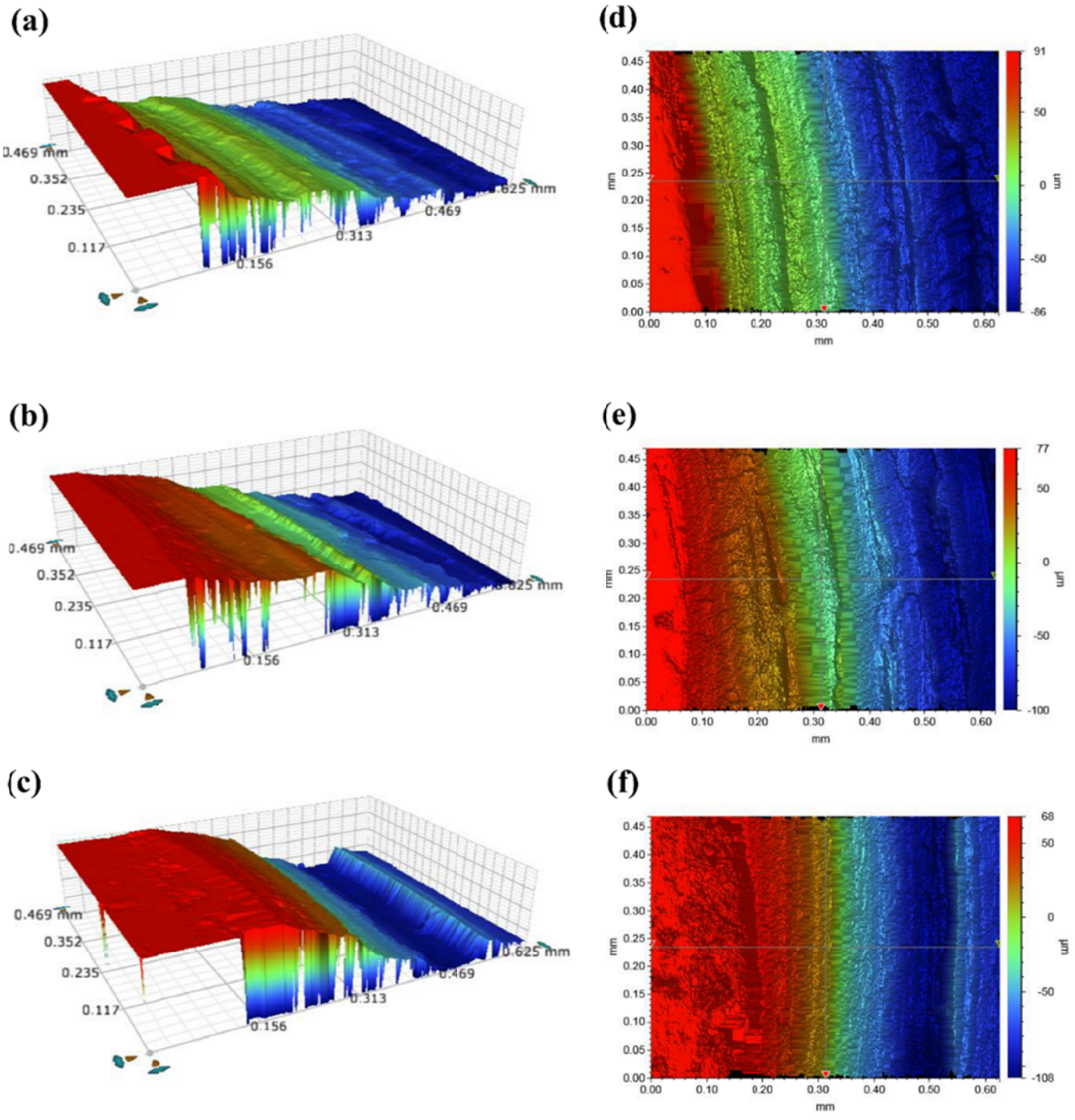

Fig. 8. 3D profiler images of the wear track: (a,d) as-built, (b,e) DA and (c,f) T6 alloys

alloy was greater compared to the other two alloys. The reason why the wear surface width of the as-built alloy was wider is suspected to be due to the debris on the wear surface described above (Fig. 7a). Debris formed during wear causes secondary wear and contributes to facilitating wear loss. In addition, it is generally believed that in sliding wear tests such as the pin-on-disc and ball-on-disc wear tests, the greater the wear properties are, the narrower the wear width becomes [24]. In other words, outstanding wear materials are likely to have grinding wear on the wear surface, and the wear width is narrower. With such characteristics, it was confirmed that the wear properties of T6 alloy are excellent. Furthermore, unlike previous studies that reported that the finer the Si particle size becomes, the more the wear property improves, this study discovered that when Si particles are at a nano-size level, they fail to execute their act as a wear resistor.

4. Conclusion

This study investigated the microstructure and room-temperature wear properties of AlSi10Mg alloy manufactured by SLM and the alloys that performed post-heat treatment (direct aging (DA), T6), and came to the following conclusions:

1. The alloy with DA heat treatment applied maintained cellular structures within molten pools, and a large number of nano-sized Si particles, which were not observed in the as-built alloy, were observed within the cellular structure. However, the molten pool and cellular structure disappeared in the T6 alloy with heat treatment applied, and coarse (μm level) Si particles were observed. In addition, the KAM value distribution was analyzed using EBSD analysis. DA alloy formed nano-sized Si particles that resulted in higher KAM values compared to the as-built alloy, and their distribution was even throughout. Meanwhile, the T6 alloy had KAM values concentrated around Si areas of the grain boundary.
2. A hardness test identified that DA alloy had a 5.2% increase in hardness compared to the as-built alloy, but in the case of the T6 alloy, the hardness decreased by 33.5%. However, a wear test measured the least wear loss in the T6 alloy, and compared to the as-built alloy, it had a 15.7% increase of wear resistance. A unique wear resistance behavior of T6 alloy was suggested.
3. The macroscopic wear surface observation of DA alloy identified cuticle-like formations on the surface, and nano-sized Si particles were found between the cuticles. Meanwhile, in the case of T6 alloy, grinding wear, which is typical in the wear surfaces of Al-Si alloys, was found. The nano-sized Si particles found in the as-built and DA alloys cause the formation of debris, and this debris causes secondary wear. In addition, the debris contributes to facilitating wear loss. Unlike this, the Si were not pulled out of the wear surface and grinding wear was observed at the wear surface in T6 alloy.

Acknowledgement

This work was supported Korea Institute for Advancement of Technology (KIAT) gran funded by the Korea Government (MOTIE) (P0002007, The Competency Development Program for Industry Specialist).

REFERENCES

[1] Y.C. Tsai, C.Y. Chou, S.L. Lee, C.K. Lin, J.C. Lin, S.W. Lim, J. Alloys Compd. **487**, 157-162 (2009).
[2] N. Read, W. Wang, K. Essa, M.M. Attallah, Mater. Des. **65**, 417-424 (2015).
[3] C.L. Xu, H.Y. Wang, F. Qiu, Y.F. Yang, Q.C. Jiang, Mater. Sci. Eng. A **417**, 275-280 (2006)
[4] T. Yu, H. Hyer, Y. Sohn, Y. Bai, D. Wu, Mater. Des. **182**, 108062,15 November 2019.
[5] J. Wu, X.Q. Wang, W. Wang, M.M. Attallah, M.H. Loretto, Acta Mater. **117**, 311-320 (2016).
[6] A. Hadadzadeh, C. Baxter, B.S Amirkhiz, M. Mohammadi, Addit. Manuf. **23**, 108-120 (2018).
[7] L. Xi, P. Wang, K.G. Prashanth, H. Li, H.V. Prykhodko, S. Scudino, I. Kaban, J. Alloys Compd. **786**, 551-556 (2019).
[8] N.T. Aboulkhair, N.M. Everitt, I. Ashcroft, C. Tuck, Addit. Manuf. **1-4**, 77-86 (2014)..
[9] I. Koutiri, E. Pessard, P. Peyre, O. Amlou, TD. Terris, J. Mater. Process. Tech. **225**, 536-546 (2018).
[10] S. Romanoa, A. Brückner-Foit, A. Brandão, J. Gumpinger, T. Ghidini, S. Beretta, Eng. Fract. Mech. **187**,65-189 (2018).
[11] J.N.D. Ngnekou, Y. Nadot, G. Henaff, J. Nicolai, W.H. Kan, J.M. cairney, L. Ridosz, Int. Jour. Fatigue **119**, 160-172 (2019).
[12] N.E. Uzan, R. Shneck, O. Yeheskel, N. Frage, Mat. Sci. Eng. A **704**, 229-237 (2017).
[13] D. Gu, H. Wang, F. Chang, D. Dai, P. Yuan, Y.C. Hagedorn, W. Meiners, Phys Procedia **56**, 108-116 (2014).
[14] N. Shivakumar, V. Vasu, N. Narasaiah, S. Kumar, Procedia Materials Science **10**, 159-167 (2015).
[15] L. Girelli, M. Tocci, M. Gelfi, A. Pola, Mat. Sci. Eng. A **739**, 371-328 (2019).
[16] P. Wei, Z. Wei, Z. Chen, J. Du, Y. He, J. Li, Y. Zhou, Appl. Surf. Sci. **408**, 38-50 (2017).
[17] A.H. Maamoun, M. Elbestawi, G.K. Dosbaevam, S.C. Veldhuis, Addit. Manuf. **21**, 234-247 (2018).
[18] B. AlMangour, M.S. Baek, D. Grzesiak, K.A. Lee, Mat. Sci. Eng. A **712**, 812-818 (2018).
[19] A. Hadadzadeh, B.S. Amirkhiz, J. Li, M. Mohammadi, Addit. Manuf. **23**, 121-131 (2018).
[20] A. Amanov, R. Umarov, Appl. Surf. Sci. **441**, 515-529 (2018).
[21] Y.J. Kang, J.H. Kim, J.I. Hwang, K.A. Lee, Trans. Mater. Process. **27**, 6, 339-346 (2018).
[22] N. Li, H. Yan, Z.W. Wang, Appl. Sci. **8**(3), 372 (2018).
[23] H.J. Kim, C.G. Kim, Journal of the Korean Foundrymen's Society **20**, 2, 89-96 (2000).
[24] N.S. Kim, K.W. Nam, J.N. Park, S.H. Ahn, H.S. Kim, J. Ocean Eng. and Technol. **24**, 6, 76-80 (2010).